Supplementary Information

Engineering of an in-cell protein crystal for fastening a metastable conformation of a target miniprotein

Mariko Kojima,[1] Satoshi Abe,[1] Tadaomi Furuta,[1] Duy Phuoc Tran,[1] Kunio Hirata,[2] Keitaro Yamashita,[2, 4] Yuki Hishikawa,[1] Akio Kitao,[1] and Takafumi Ueno[*,1,3]

[1]School of Life Science and Technology, Tokyo Institute of Technology, Nagatsuta-cho 4259, Midori-ku, Yokohama 226-8501, Japan

[2]SR Life Science Instrumentation Unit, RIKEN/SPring-8 Center, 1-1-1, Kouto, Sayo-cho, Sayo-gun, Hyogo 679-5148, Japan

[3]International Research Frontiers Initiative (IRFI), Tokyo Institute of Technology, Nagatsuta-cho 4259, Midori-ku, Yokohama 226-8501, Japan

[4]MRC Laboratory of Molecular Biology, Francis Crick Avenue, Cambridge CB2 0QH, UK

Corresponding Author

*Email: tueno@bio.titech.ac.jp

Table of Contents

Experimental Procedures

Materials

The *Spodoptera frugiperda* insect cell line IPLB-Sf21-AE (Sf21) was maintained in tissue culture flasks in Grace's medium (Gibco–BRL) at 27 °C with 10% fetal bovine serum (MP Biomedicals. Inc.), 2.6 mg/mL tryptose broth, 100 U/mL penicillin, and 100 μg/mL streptomycin. Sf21 cells in Sf-900™ III SFM and DH10Bac™ Cells were purchased from Thermo Fisher Scientific. The competent cells of DH5α *E. coli* and DH10Bac *E. coli* were purchased from Toyobo and InvitrogenTM (Life Technologies). The PCR reactions were implemented using QuikChange® Site-Directed Mutagenesis Kit (Stratagene) and KOD Plus Mutagenesis Kit (Toyobo). Other reagents were purchased from TCI, Wako, Nacalai Tesque, Sigma–Aldrich, and Life Technologies and were used without further purification.

Preparation of mutant PhCs

The plasmid DNAs of **1-PhC**, **2-PhC**, **3-PhC**, **4-PhC**, and **2-PhC^{D74R}** were prepared by inverse PCR using wild-type PhC in pFastBac™ vector as a template. This was amplified with DH5α (Toyobo) and extracted with the QIAprep Spin Miniprep Kit (QIAGEN). The plasmids were transformed into DH10Bac™ Cells, where the baculovirus shuttle vector (bacmid) is present, and incubated with ampicillin, kanamycin, and gentamicin to generate recombinant bacmids by transposing Tn7 element from a pFastBac™ donor plasmid to the mini-*att*Tn7 attachment site on the bacmid. Expression of these mutant PhCs in insect cells was performed according to previous literature.[1] The purified recombinant bacmid DNAs were transfected to Sf21 cells with CellfectinII reagent and incubated at 27 °C for 6 hours with Grace's medium. After 6 hours, Grace's medium was changed to Grace's medium with 10% fetal bovine serum and incubated at 27°C for 4 days. The supernatant of the medium containing the mutant baculovirus was used for expression in the insect cell, Sf21. Expression of mutants was performed by the same procedures with Wild type PhC (WT-PhC). Cells were lysed with RIPA buffer containing SDS, and the crystals were purified by sonication and centrifugation.

SEM analysis

SEM analyses of mutant PhCs were performed on field-emission scanning electron microscopy (FE-SEM, Hitachi S-5500) after treatment of the sample with platinum coater (Hitachi, MC1000). SEM images show that **1-PhC**, **3-PhC**, **4-PhC**, and **2-PhC^{D74R}** were cubic, missing diagonal vertex, and **2-PhC** is a tetrahedral crystal (Fig. S2).

X-ray crystal structure analysis

Sf21 cells including crystals were immersed in Grace medium containing 50% (v/v) ethylene glycol, spread over MicroMesh, and frozen in liquid nitrogen. The X-ray diffraction data of each crystal were collected at 100K at the beamline BL32XU at SPring-8 using an X-ray wavelength of 1.00 Å. The whole data collection process was automated by *ZOO* system including sample exchange by the robot.[2] Serial Synchrotron Rotation Crystallography (SS-ROX) method, which was developed to collect diffraction data of microcrystals efficiently, was employed.[3, 4] A microbeam of 1.2 μm (vertical) x 1.0 μm (horizontal) was used. The datasets were collected using a helical rotation of 0.25° and translation of 1μm per frame with a frame rate of 58.824 Hz (~2 x 10^{10} photons/frame). The index was performed using *CrystFEL* version 0.6.3 with *Dirax* and *Mosflm*.[5-7] The number of indexed images for **1-PhC**, **2-PhC**, **3-PhC**, **4-PhC**, and **2-PhC^{D74R}** are 20752, 8616, 59747, 6616, and 9607, respectively. Integrated intensities were merged by process_hkl in the *CrystFEL* suite. The structure was solved by rigid body refinement with phenix.refine using the previously solved structure (5GQM).[8] Refinement of the protein structure was performed at resolutions of 1.65 Å, 1.55 Å, 1.75 Å, 1.70 Å, 1.85 Å, and 1.70Å for **1-PhC**, **2-PhC**, **3-PhC**, **4-PhC**, **2-PhC^{D74R}**, respectively, using REFMAC5 in the of CCP4 suite.[8] Rebuilding was performed using COOT based on sigma-A weighted $2|F_o|-|F_c|$ and $|F_o|-|F_c|$ electron density maps. The Y71(Y2)–W78(W9) in **1-PhC**, Y71–H84 in **3-PhC**, A72–S89 in **4-PhC**, and Y72(Y1)–S84 in **2-PhC^{D74R}** could not be modeled because electron densities corresponding to these residues were missing.[9] The side chain of W80(W9) in **2-PhC** could not be modeled because of the disordered electron densities of the side chain. The models were subjected to quality analysis during the various refinement stage with omit maps and RAMPAGE.[10]

The diffraction and refinement statistics are summarized in Table S1. Atomic coordinates for **2-PhC** within cell have been deposited in the Protein Data Bank under accession codes 7WYR. All images were produced using PyMOL (https://pymol.org/).

Molecular dynamics simulation

The initial structures of the isolated **CLN025$^{2\text{-PhC}}$** fragment, the monomer, and the trimer of **2-PhC** (**2-PhM** and **2-PhT**, respectively) were constructed from the crystal structure of **2-PhC** (PDB ID: 7WYR), and that of **2-PhT^{D74R}** was constructed from **2-PhT** by mutating D74(D3) to arginine with PyMOL. The nucleotides were removed from all structures. Counter ions (Na^+ and Cl^-) were added to preserve electric neutrality. For each system, the energy minimization of 300 steps was carried out with restraints on heavy atoms. Then, 500 ps equilibration under NVT condition (300 K) and 500 ps equilibration under NPT condition (300 K and 1 bar) were conducted with the same restraints above. Finally, 300 ns production runs were conducted for all systems without restraints. In the isolated system and **2-PhM**, three runs were conducted with different initial velocities using random seeds. All the MD simulations were performed using the Amber ff14SB force field and TIP3P water model.[11, 12] The temperature and pressure were regulated by the Berendsen thermostat and barostat, respectively. The time step was set to 2 fs, and the trajectories were recorded every 1 ns. The MDTraj software was used to analyze the RMSD, dihedral angles, and distances.[13] PyMOL was used for visualization of the structures.

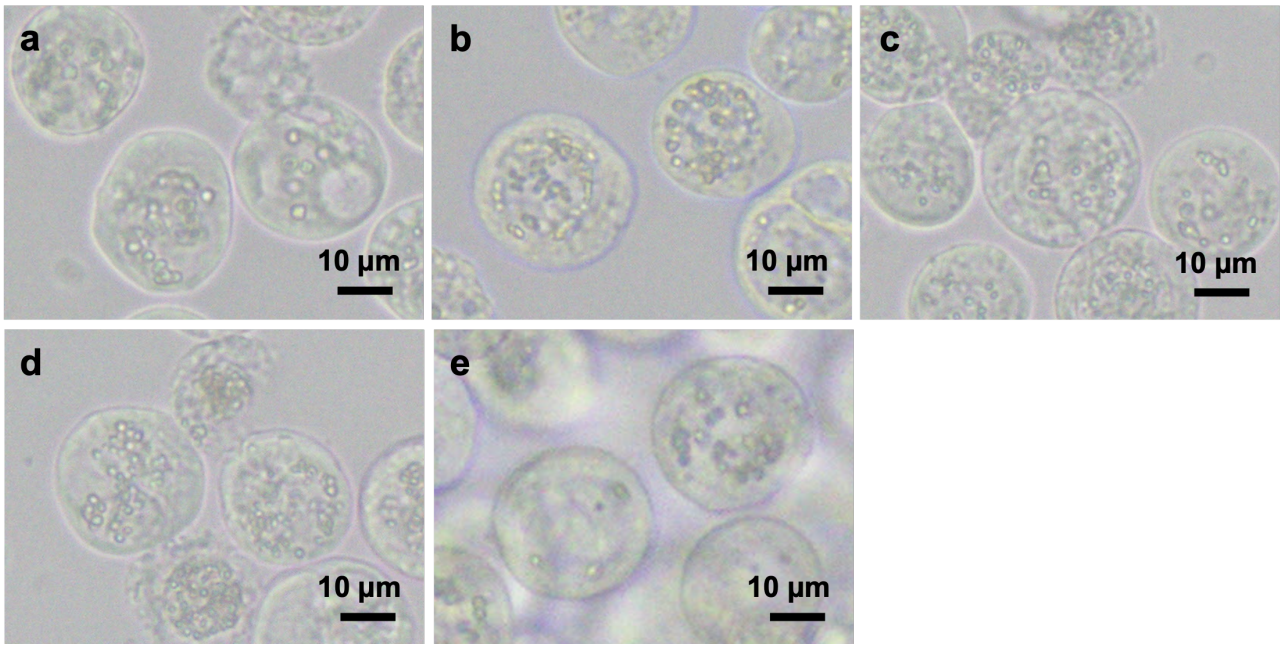

Fig. S1 Inverted microscope images of (a) **1-PhC**, (b) **2-PhC**, (c) **3-PhC**, (d) **4-PhC** and (e) **2-PhC**^{D74R} in Sf21.

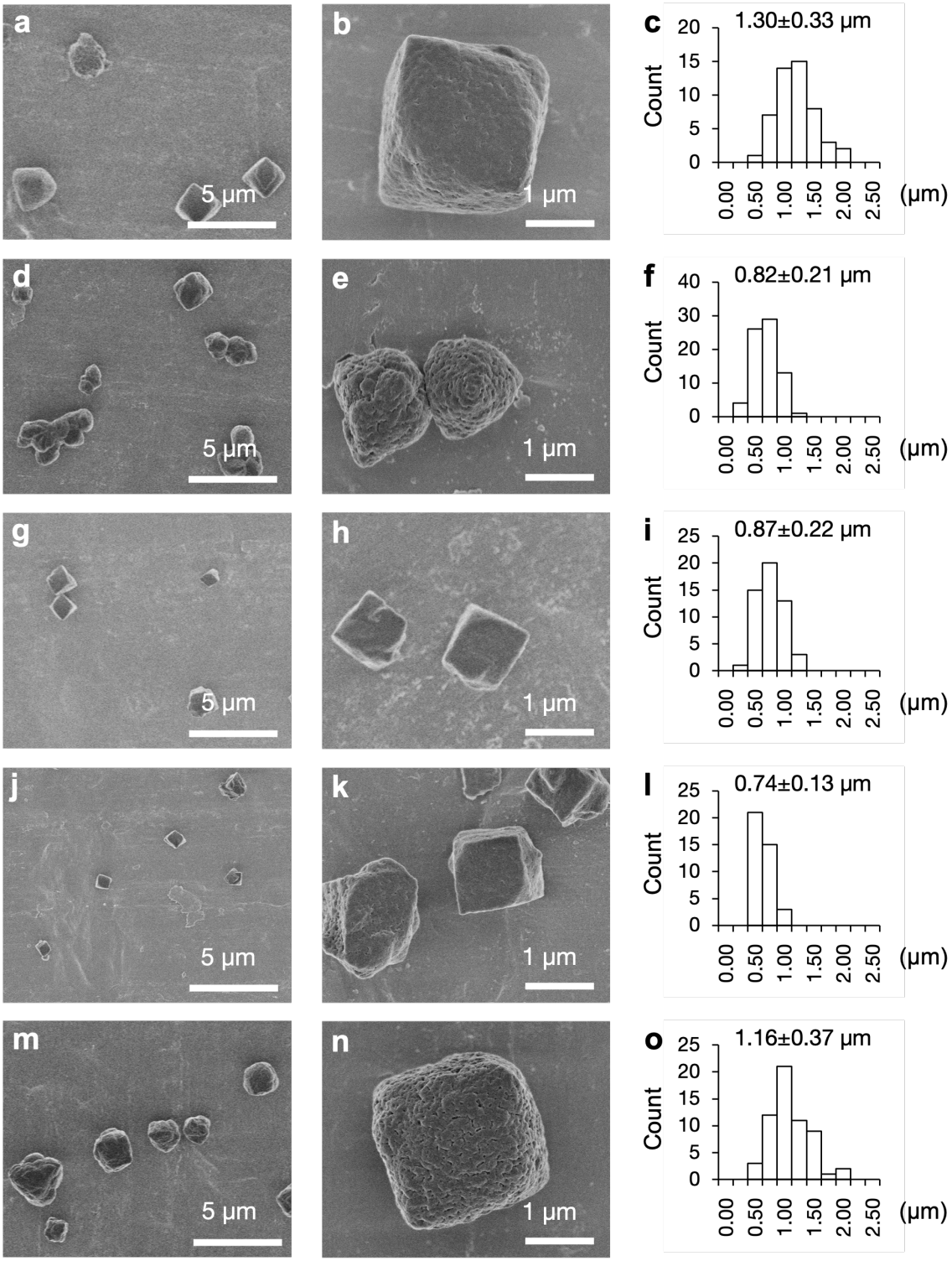

Fig. S2 SEM images and size histogram of (a-c) **1-PhC**, (d-f) **2-PhC**, (g-i) **3-PhC**, (j-l) **4-PhC** and (m-o) **2-PhC^{D74R}.** Average size of each mutant crystal is on top of the histogram.

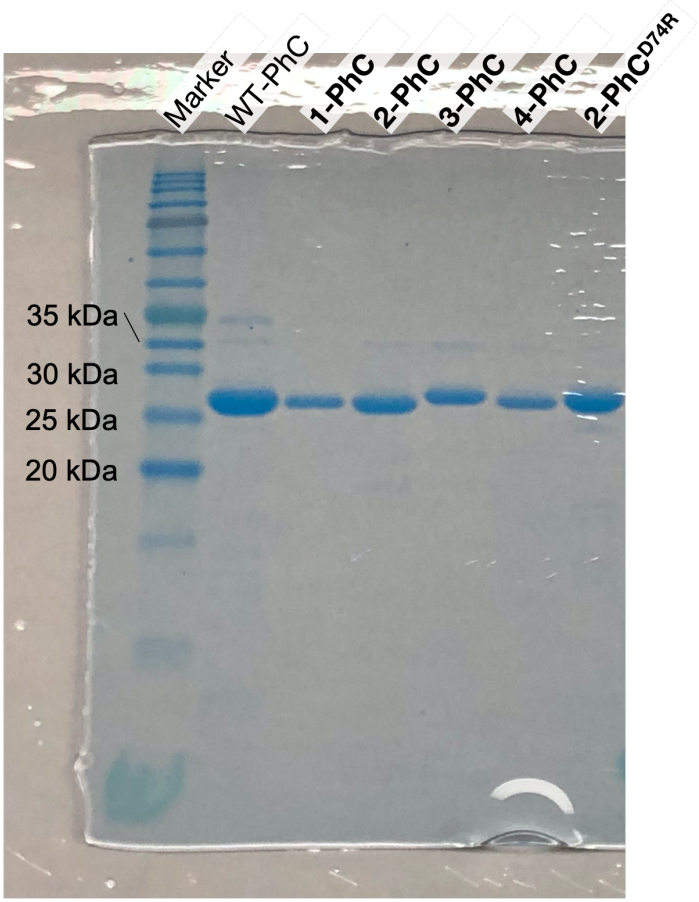

Fig. S3 SDS-PAGE of WT-PhC, **1-PhC**, **2-PhC**, **3-PhC**, **4-PhC** and **2-PhC^{D74R}**. Weak intensity bands around 35 kDa on all lanes are impurities.

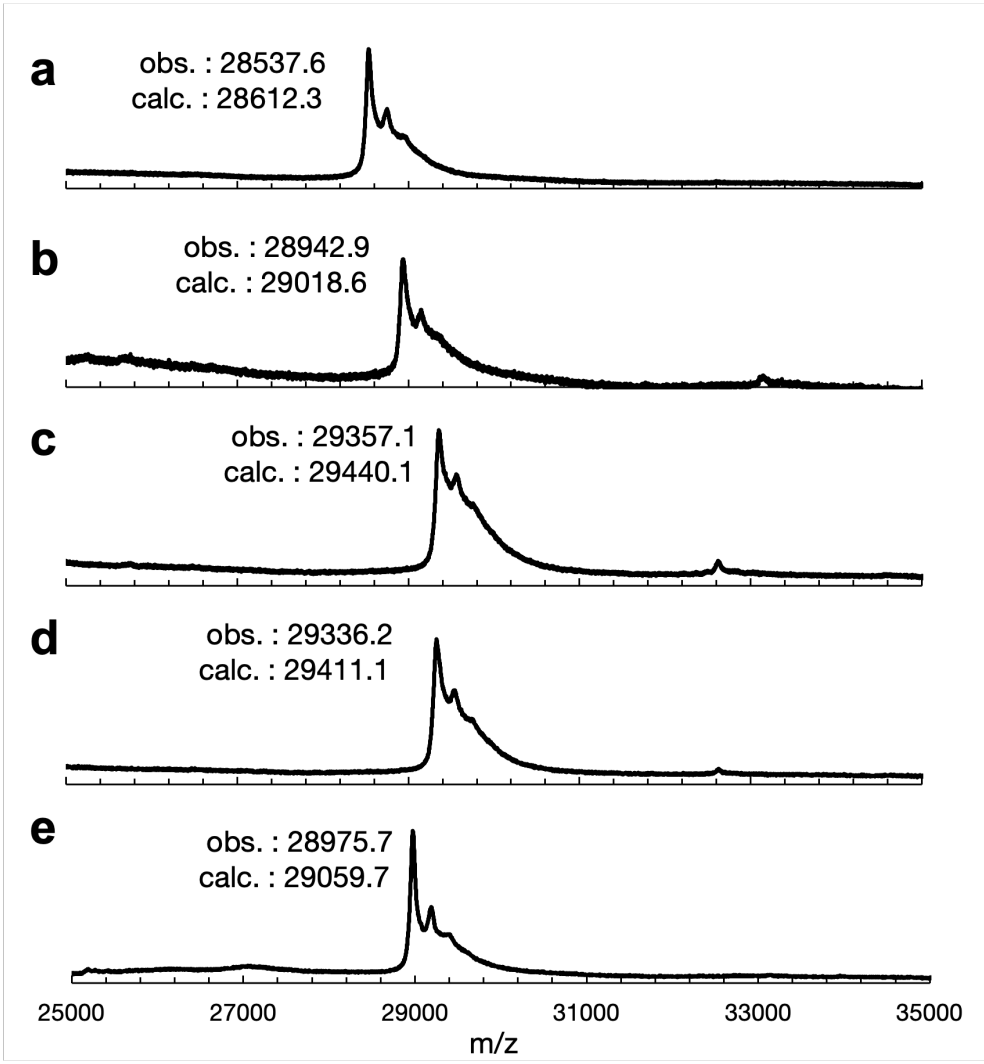

Fig. S4 MALDI-TOF-MS of (a) **1-PhC**, (b) **2-PhC**, (c) **3-PhC**, (d) **4-PhC** and (e) **2-PhC**^{D74R}.

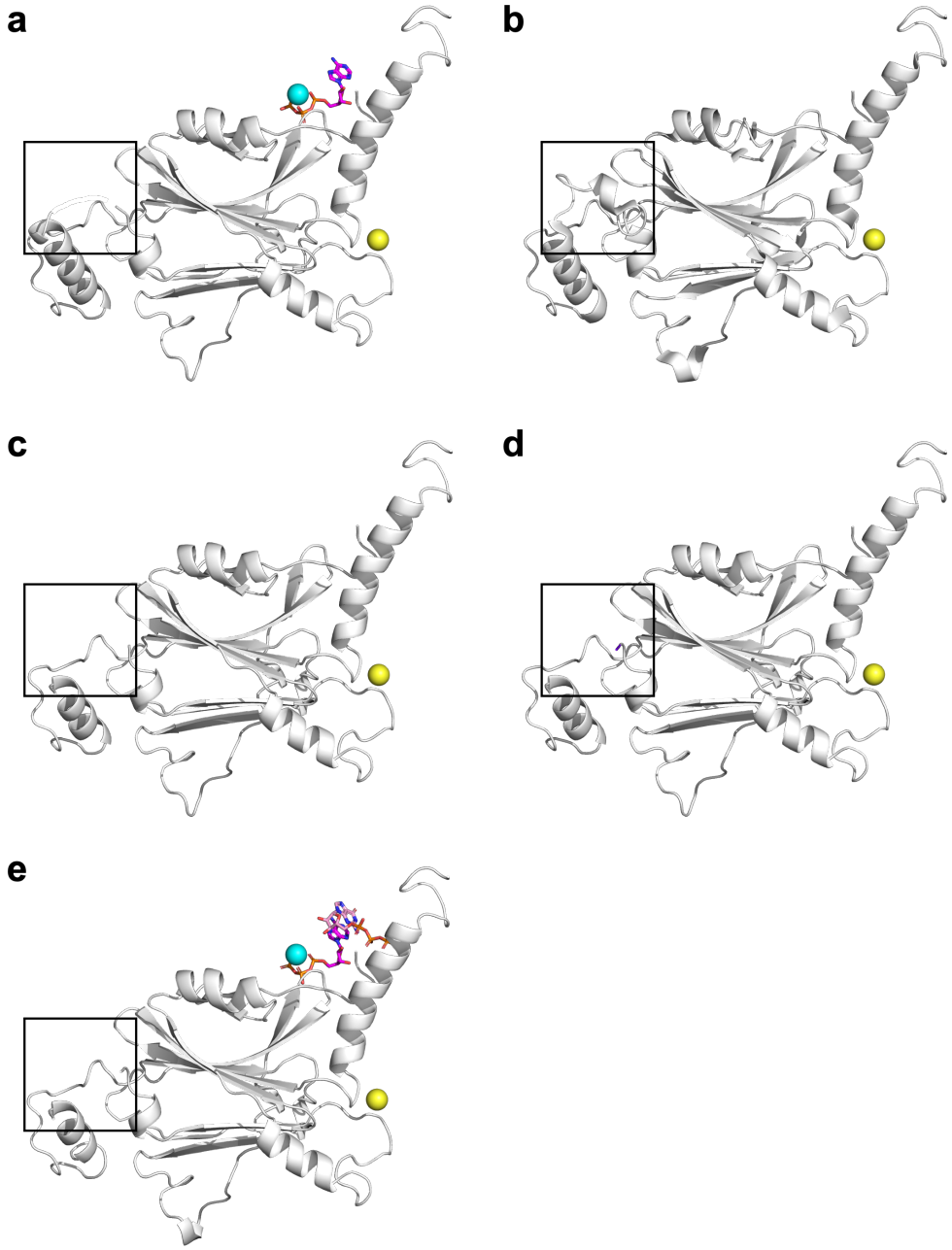

Fig. S5 The structures of (a) **1-PhM**, (b) **2-PhM**, (c) **3-PhM**, (d) **4-PhM**, and (e) **2-PhM^{D74R}**. Black square shows the position of the inserted CLN025. ATP and GTP are displayed as stick colored in magenta and pink, respectively. Chloride ion and magnesium ion are displayed as spheres colored in yellow and cyan, respectively. N, O, and P atoms are colored in blue, red, and orange, respectively.

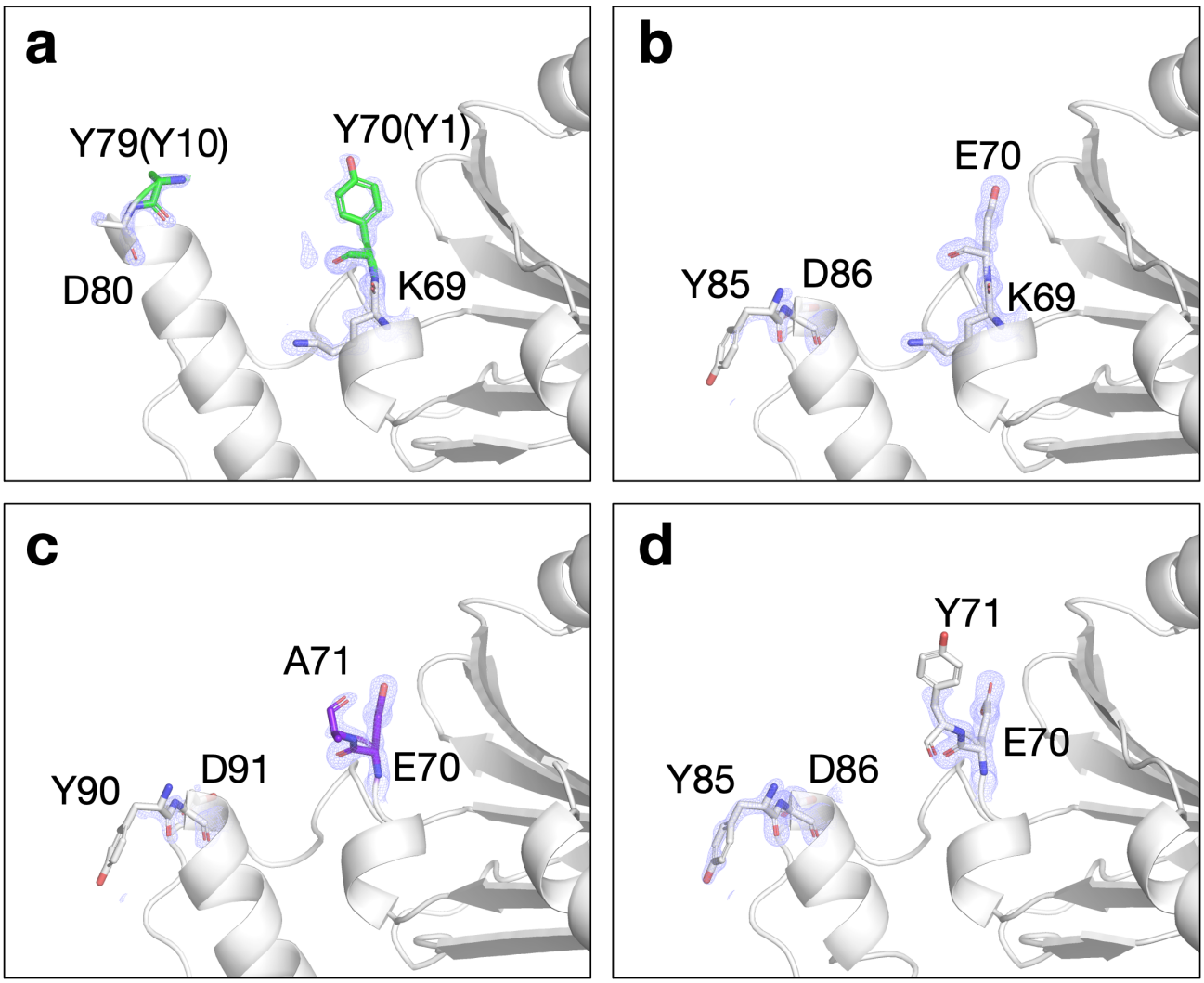

Fig. S6 Close-up views of CLN025 fusion site in (a) **1-PhC**, (b) **3-PhC**, (c) **4-PhC**, (d) **2-PhM^{D74R}**. Green sticks show inserted CLN025. Purple sticks show EAAK linker inserted between PhM and CLN025. The selected 2|Fo|−|Fc| electron density maps at 1.0σ are shown in blue. N, O, and P atoms are colored in blue, red, and orange, respectively. Y79(Y10) and D80 in (a) was replaced by alanine because of the low electron density corresponding to side chains.

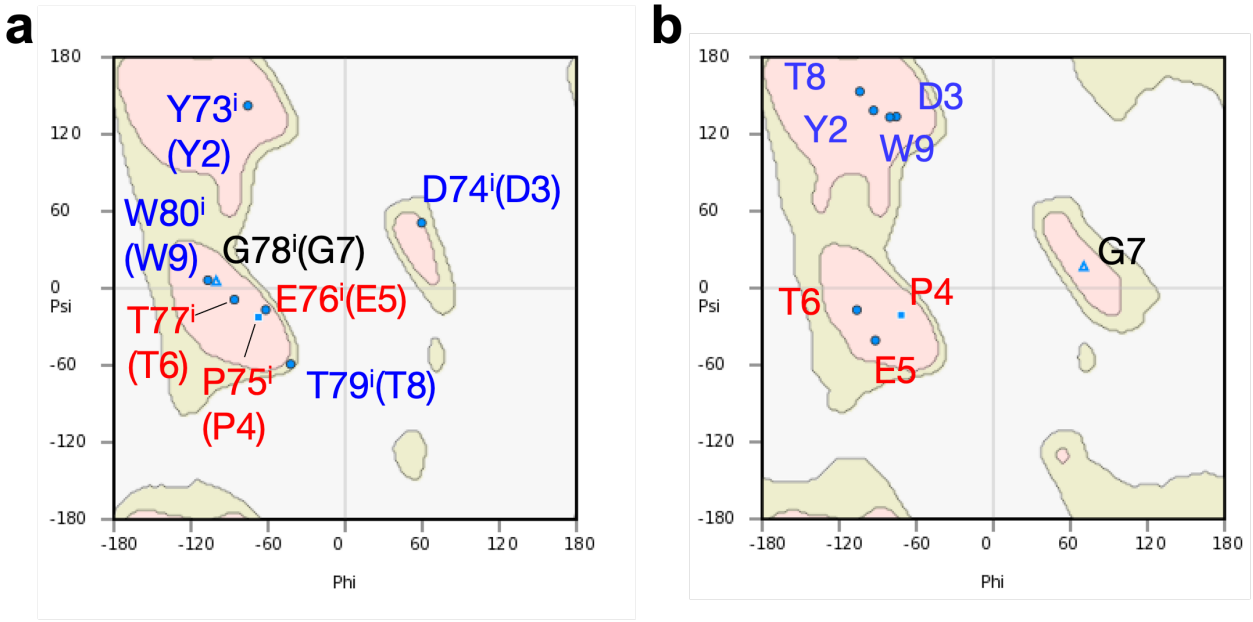

Fig. S7 Ramachandran plot of (a) Y73^{i}(Y2)–W80^{i}(W9) of **2-PhC** and (b) Y2–W9 of CLN025^{5AWL}. COOT was used to calculate the distributions of backbone dihedral angles across all residues.[9] Triangle and square dots mean glycine and proline, respectively. The other residues are displayed as circular dots.

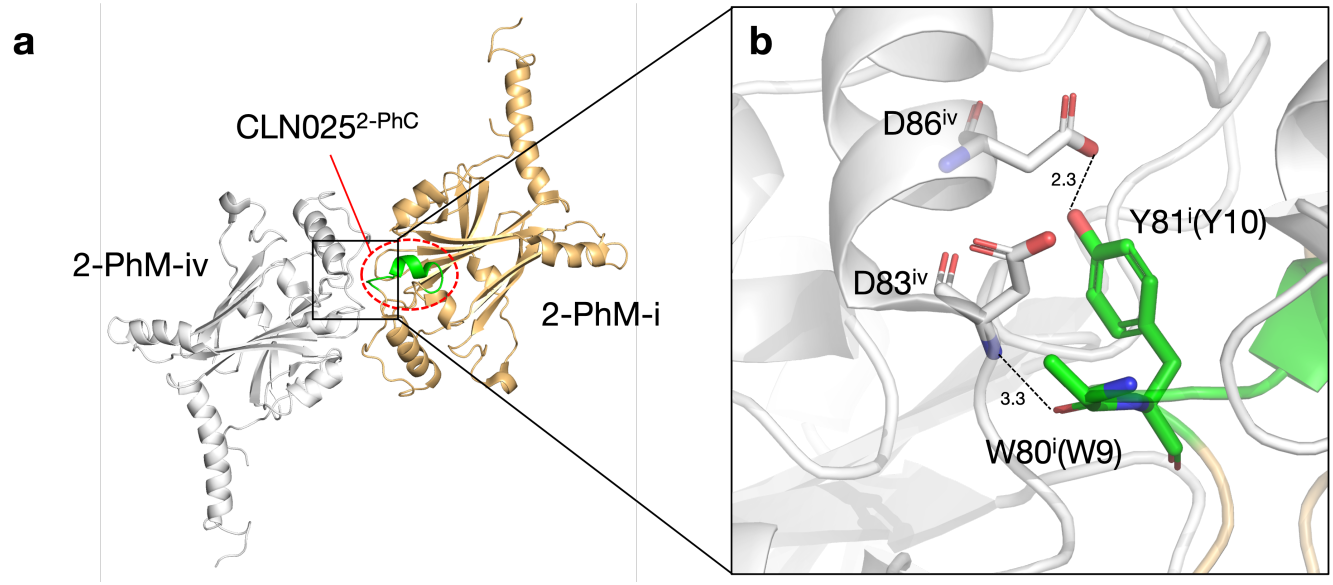

Fig. S8 The crystal structure of **2-PhC**. (a) Contact of **2-PhM-i** and **2-PhM-iv** at the interface of two trimers of **2-PhC**. (b) Intermolecular interactions of the assigned CLN025 fragment at W80^{i}(W9) and Y81^{i}(Y10) in **2-PhC**. The amino acids of the CLN025 fragments were shown in green. W80^{i}(W9) is replaced with alanine residue because of the disordered electron densities of the side chain. N and O atoms are colored in blue and red, respectively. The hydrogen bonds are shown as black dashed lines.

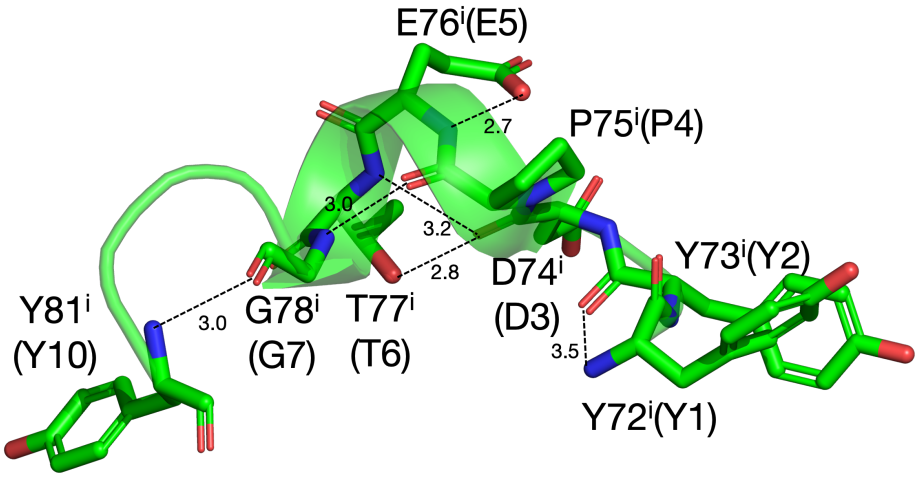

Fig. S9 Interactions within the **CLN025$^{2\text{-PhC}}$** fragment. The amino acids of the CLN025 fragments were shown in green. N and O atoms are colored in blue and red, respectively. The hydrogen bonds are shown as black dashed lines.

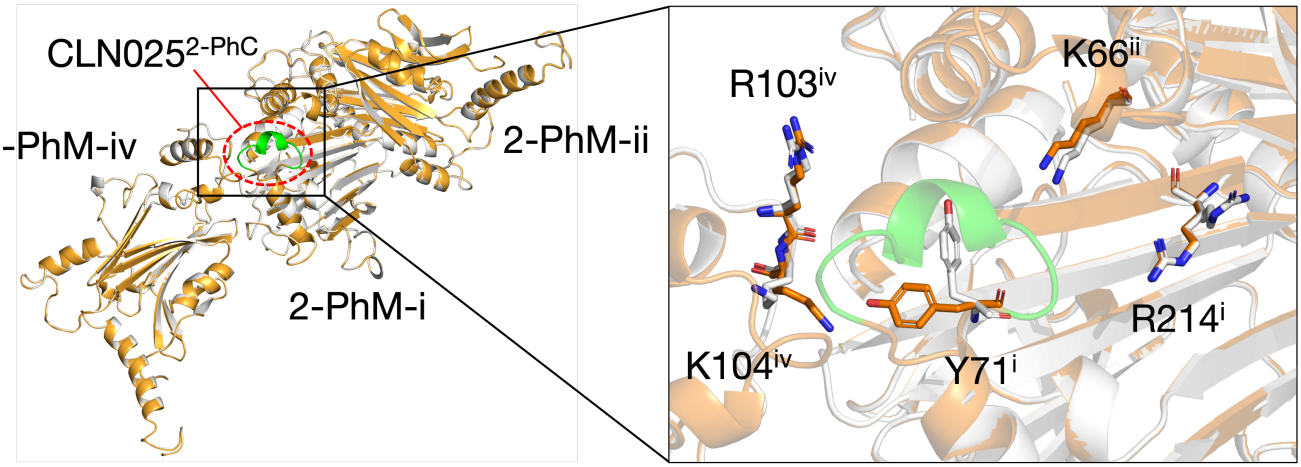

Fig. S10 The overlayed structures of **2-PhC** and **2-PhC^{D74R}** around CLN025 inserted region. **2-PhC** and **2-PhC^{D74R}** were colored in orange and gray, respectively. The amino acids of the CLN025 fragments were shown in green. N and O atoms are colored in blue and red, respectively.

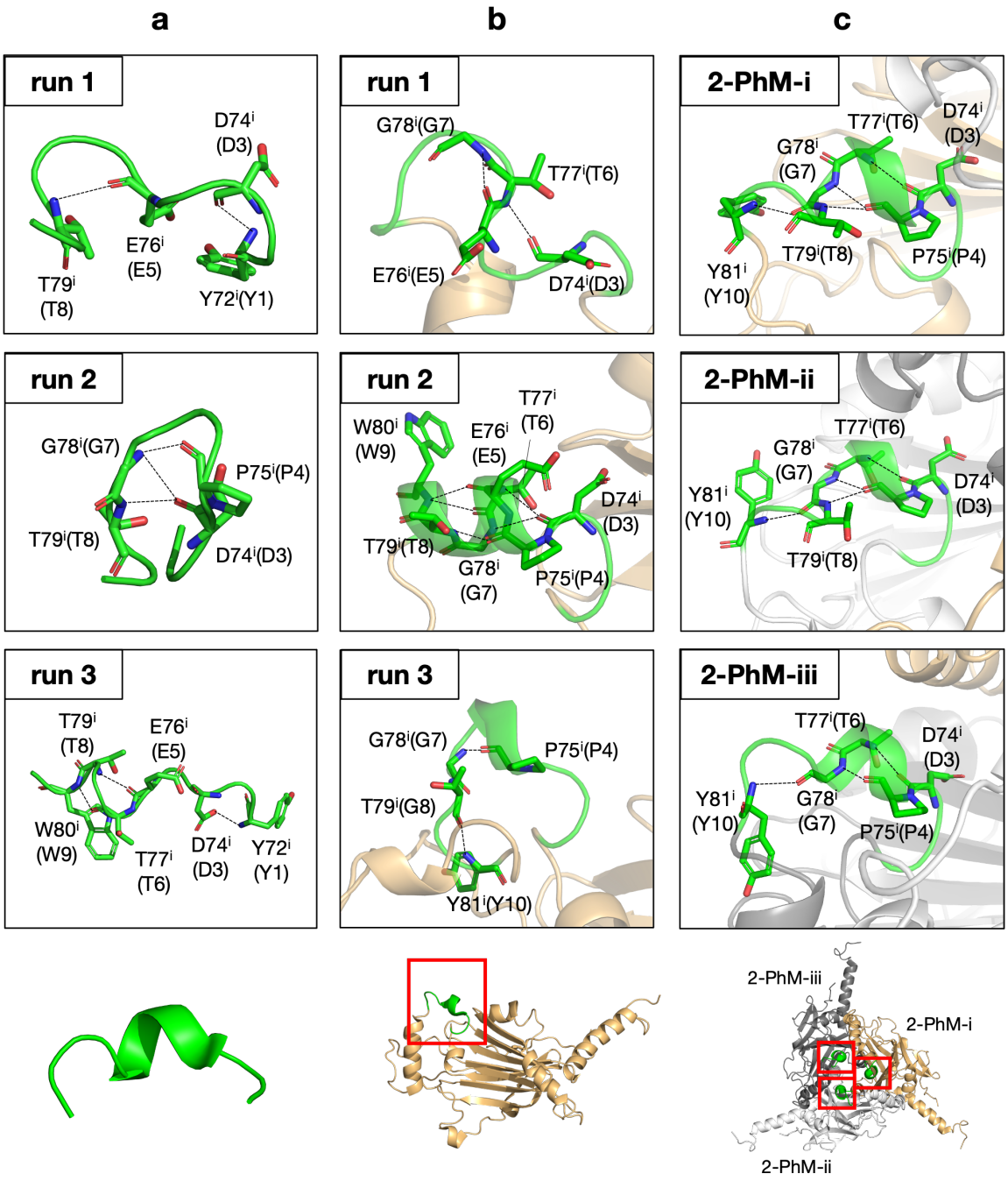

Fig. S11 Structures of (a) the isolated **CLN025$^{2\text{-PhC}}$** fragment and (b,c) the **CLN025$^{2\text{-PhC}}$** fragments in (b) **2-PhM** and (c) **2-PhT** at the 300 ns of the MD simulations. Structures after 300 ns of three runs, run 1, 2, and 3, and three monomers, **2-PhM-i**, **-ii**, and **-iii**, were shown. The initial structures of each system were shown at the bottoms of the images. The amino acids of the CLN025 fragments were shown in green. Red squares show the position of the CLN025 fragments. N and O atoms are colored in blue and red, respectively. The main-chain hydrogen bonds with the distance less than 3.5 Å are shown as black dashed lines.

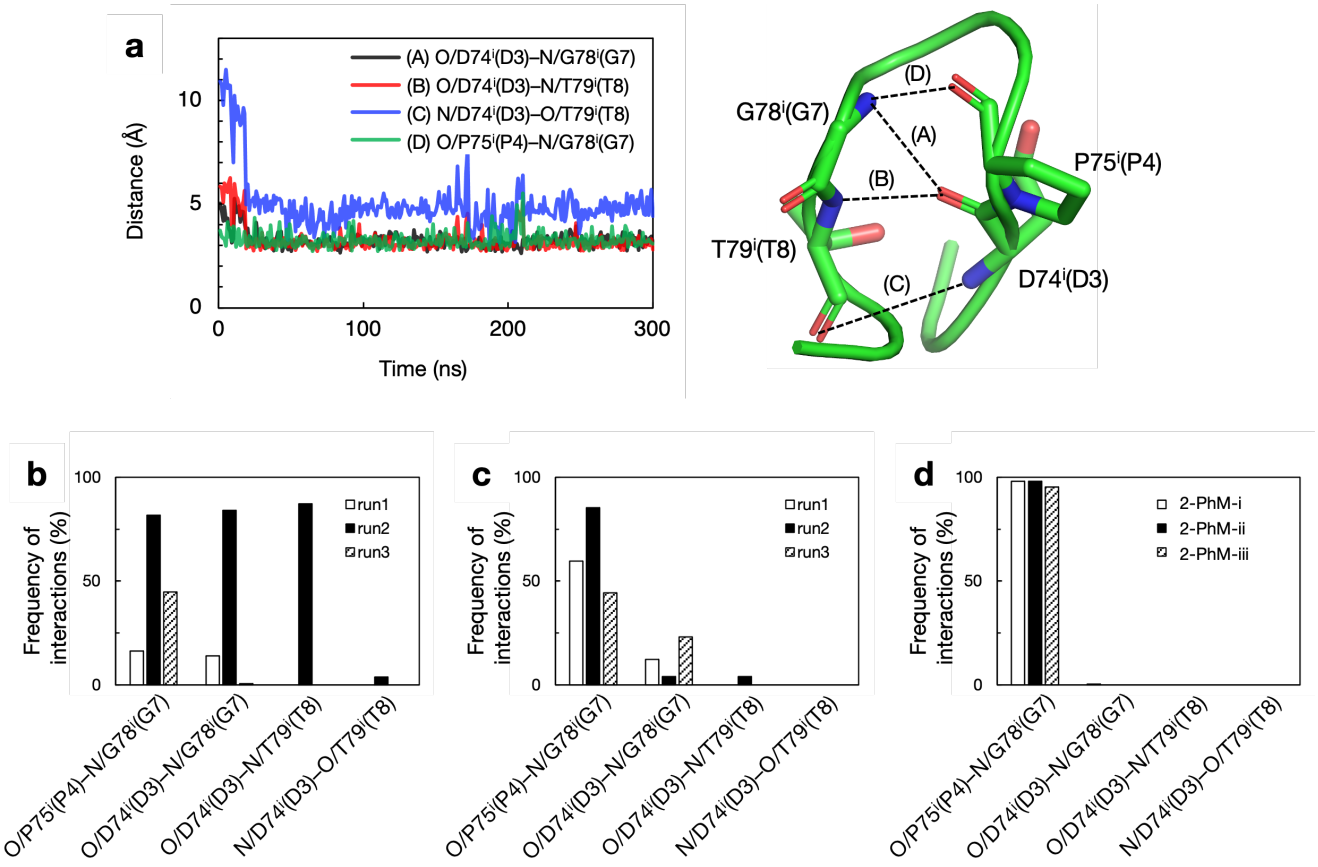

Fig. S12 The time courses of the distances and the frequency of four intramolecular interactions within CLN025 fragment during 300 ns MD. (a) The time courses of the distances of intramolecular interactions of **CLN025$^{2\text{-PhC}}$** during 300 ns MD simulation of run2. The positions of each interaction were shown in the right structure of the **CLN025$^{2\text{-PhC}}$** fragment at 300 ns of run2. (b-d) The frequency of four intramolecular hydrogen bonds in (b) **CLN025$^{2\text{-PhC}}$** (isolated), (c) the **CLN025$^{2\text{-PhC}}$** fragments of **2-PhM** (monomer), and (d) the **CLN025$^{2\text{-PhC}}$** fragments of **2-PhT** (trimer). N and O atoms are colored in blue and red, respectively. Data from three runs, run 1, 2, and 3, for the **CLN025$^{2\text{-PhC}}$** fragment and **2-PhM** and that from 3 monomers, **2-PhM-i**, **-ii**, and **-iii**, in **2-PhT** and **2-PhT^{D74R}** were colored in different patterns. The frequency means the percentage of coordinates in which hydrogen bonds were formed to 300 coordinates extracted from MD every 1 ns. Cut-of values of hydrogen bonds were 3.5 Å.

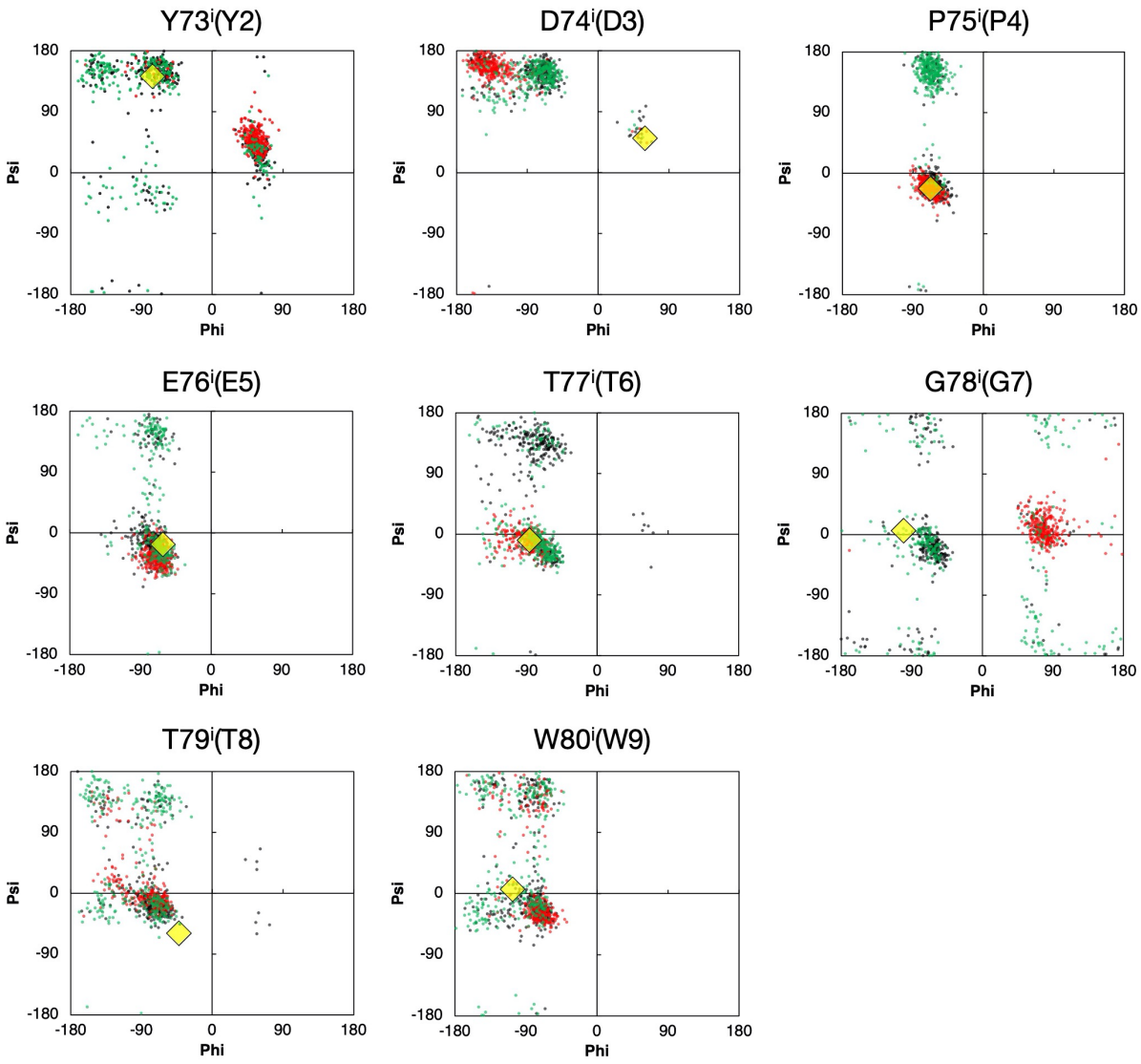

Fig. S13 The distribution of dihedral angles of Y73^{i}(Y2)–W80^{i}(W9) of the **CLN025$^{2\text{-PhC}}$** fragment in MD simulation. The distributions of three runs, run 1, 2, and 3, were colored in black, red, and green, respectively. The initial dihedral angles were pointed by yellow rhombus.

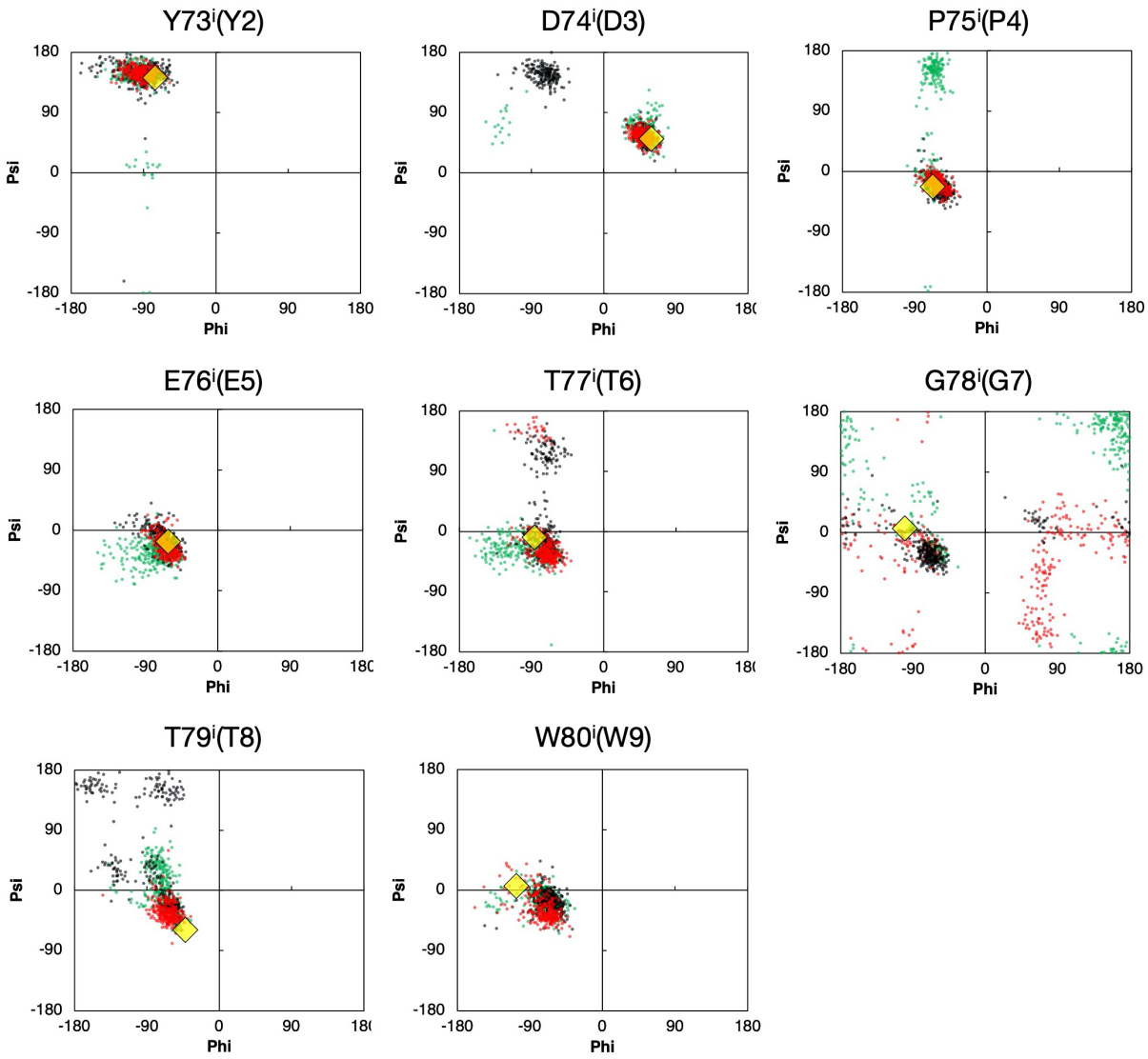

Fig. S14 The distribution of dihedral angles of Y73^{i}(Y2)–W80^{i}(W9) of **CLN025$^{2\text{-PhC}}$** in **2-PhM** in MD simulation. The distributions of three runs, run 1, 2, and 3, were colored in black, red, and green, respectively. The initial dihedral angles were pointed by yellow rhombus.

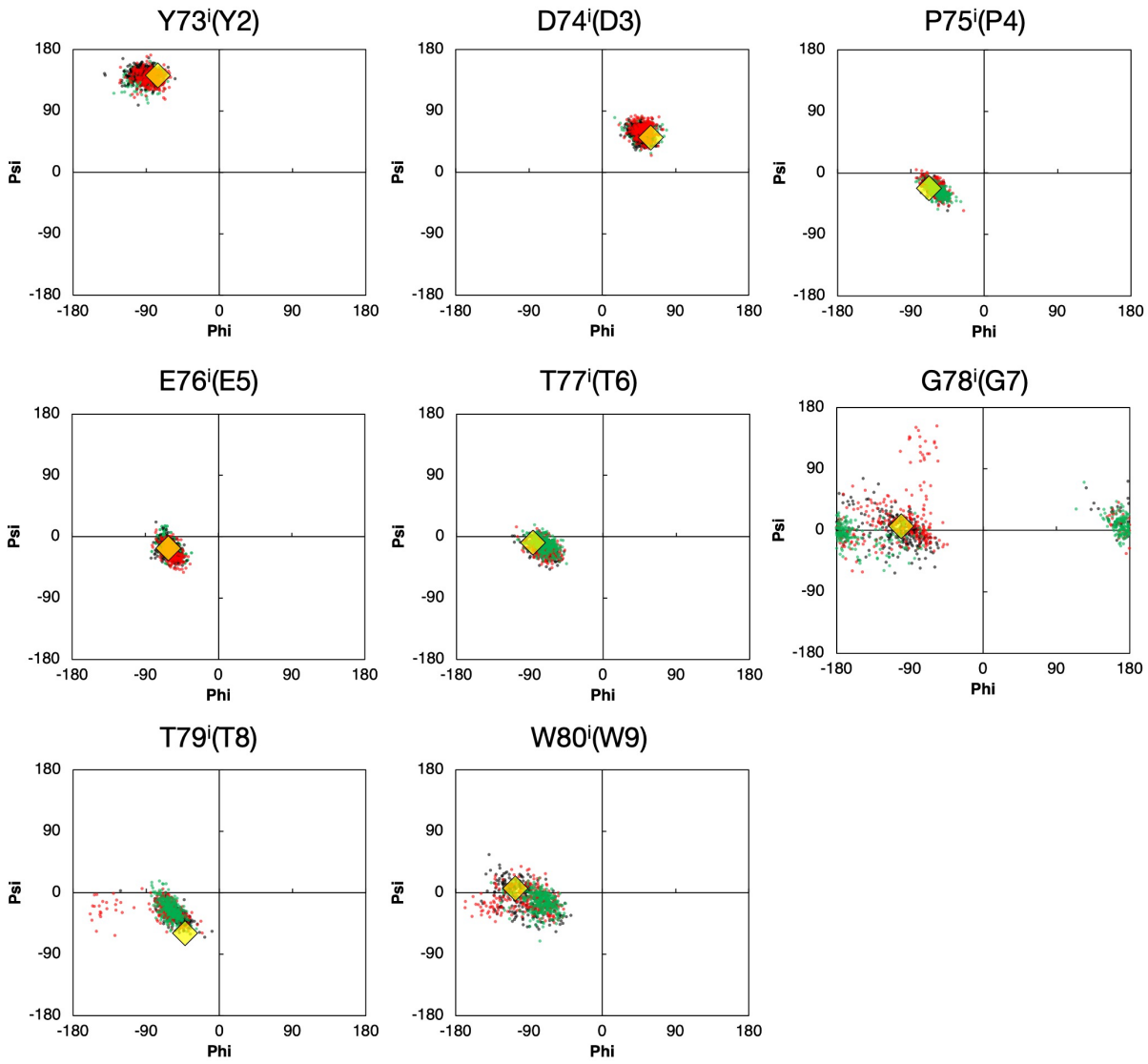

Fig. S15 The distribution of dihedral angles of Y73^{i}(Y2)–W80^{i}(W9) of **CLN025$^{2\text{-PhC}}$** in **2-PhT** in MD simulation. The distributions of three monomers, **2-PhM-i**, **-ii**, and **-iii**, were colored in black, red, and green, respectively. The initial dihedral angles were pointed by yellow rhombus.

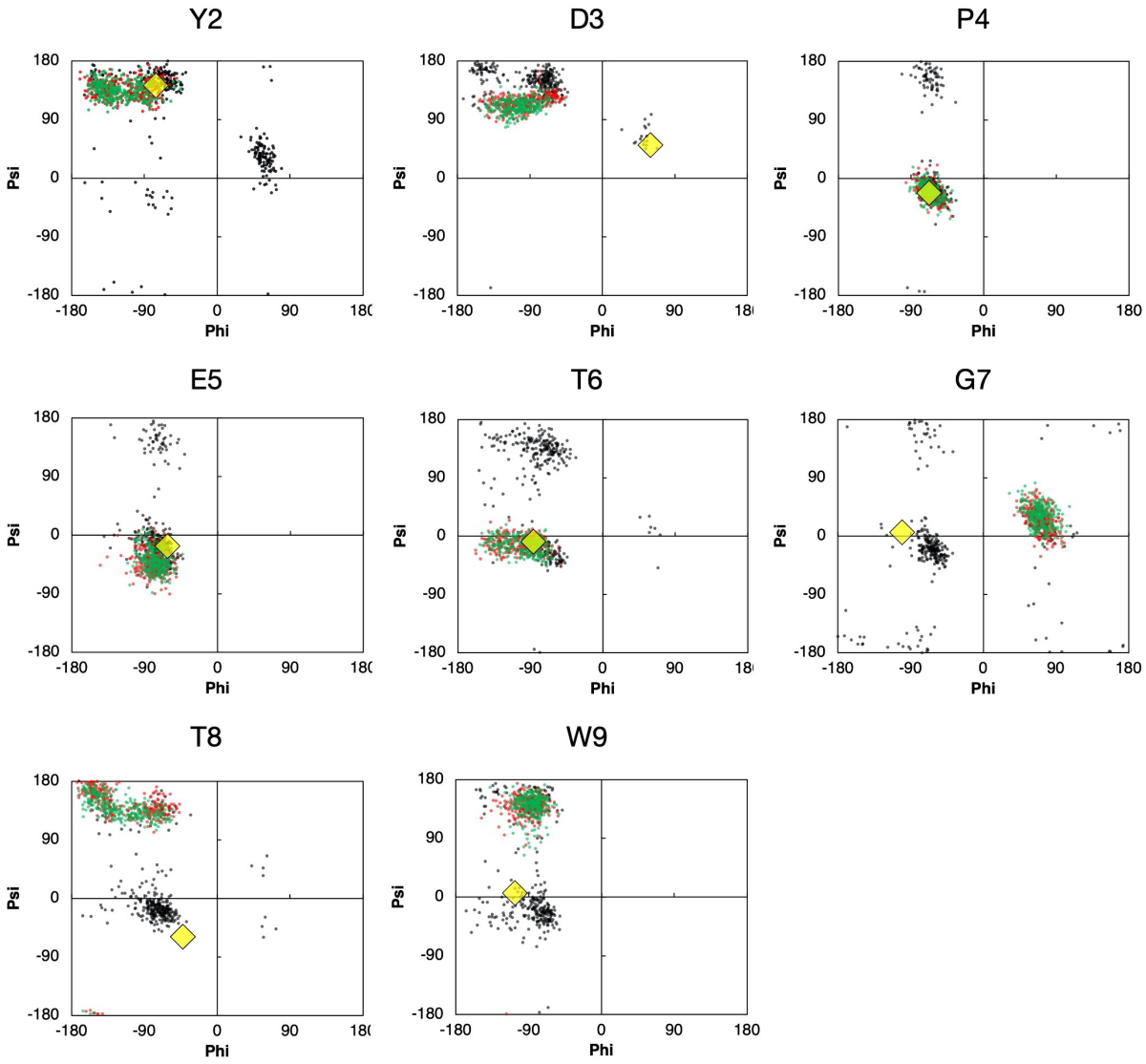

Fig. S16 The distribution of dihedral angles of Y2–W9 of CLN025^{5AWL} fragment in MD simulation. The distributions of three runs, run 1, 2, and 3, were colored in black, red, and green, respectively. The initial dihedral angles were pointed by yellow rhombus.

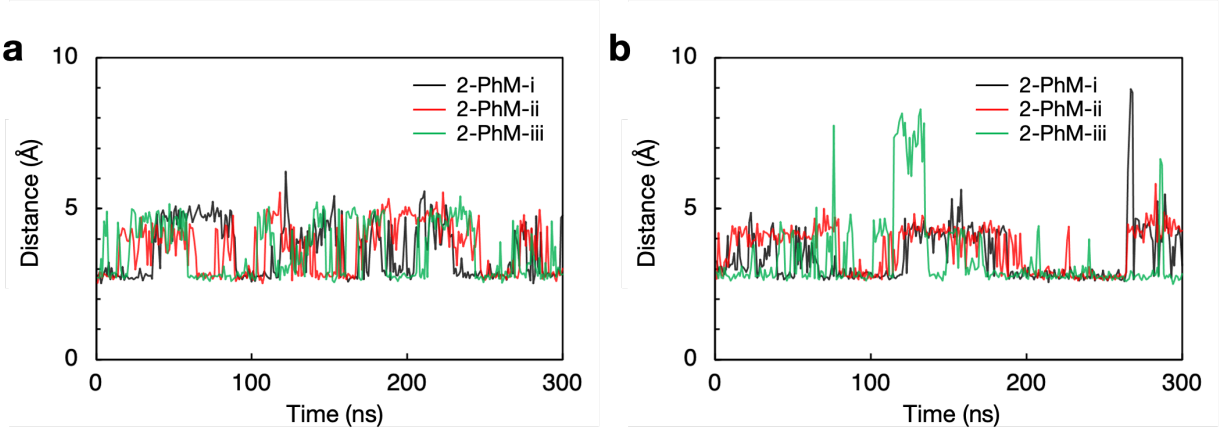

Fig. S17 The time courses of the distances at (a) Oδ1/D74^{i}(D3)–Nζ/K66^{ii} and (b) Oε1/E76^{i}(E5)–Nζ/K66^{ii} of **2-PhT**. Data from three monomers, **2-PhM-i**, **-ii**, and **-iii**, in **2-PhT** were colored in black, red, and green, respectively.

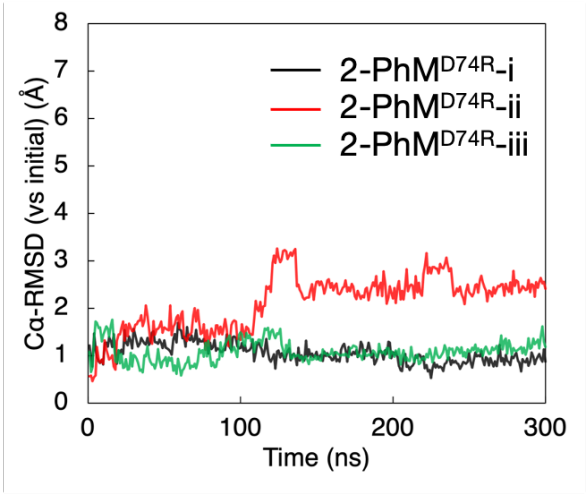

Fig. S18 The time courses of the Cα-RMSD of the **D74R-CLN025** fragments in **2-PhT^{D74R}** (mutant trimer) from the initial structures. Data from each monomer, **2-PhM^{D74R}-i**, **-ii**, and **-iii**, in **2-PhT^{D74R}** were colored in black, red, and green, respectively.

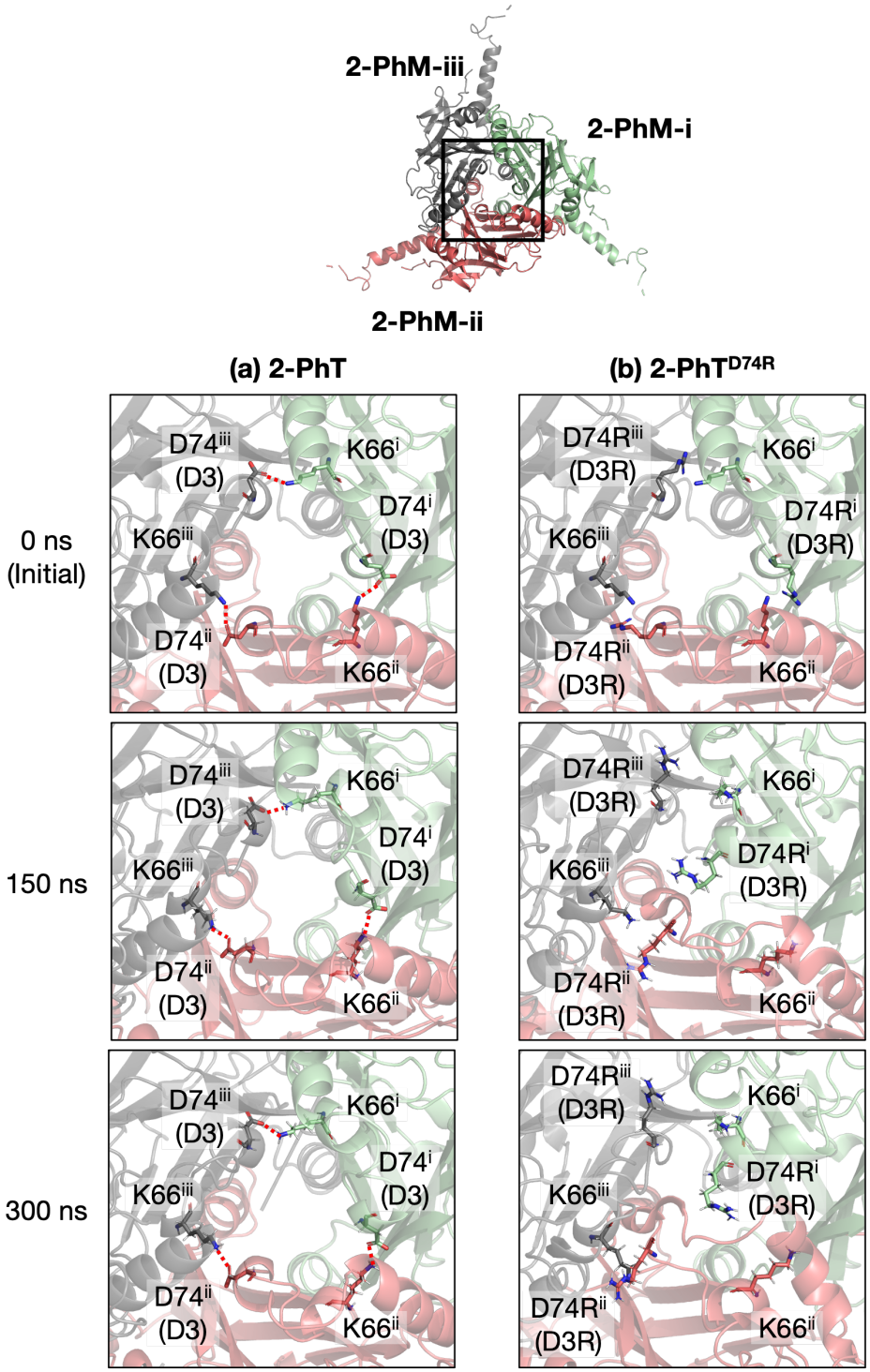

Fig. S19 The trace of structural change of interactions at (a) $D74^{i}$(D3)–$K66^{ii}$, $D74^{ii}$(D3)–$K66^{iii}$, and $D74^{iii}$(D3)–$K66^{i}$ in **2-PhT** and (b) $D74R^{i}$(D3R)–$K66^{ii}$, $D74R^{ii}$(D3R)–$K66^{iii}$, and $D74R^{iii}$(D3R)–$K66^{i}$ in **2-PhT^{D74R}**. Three monomers in trimer, **2-PhM-i**, **-ii**, and **-iii** were colored in green, red, and black, respectively. Red dotted lines show the salt bridge formation. N and O atoms are colored in blue and red, respectively.

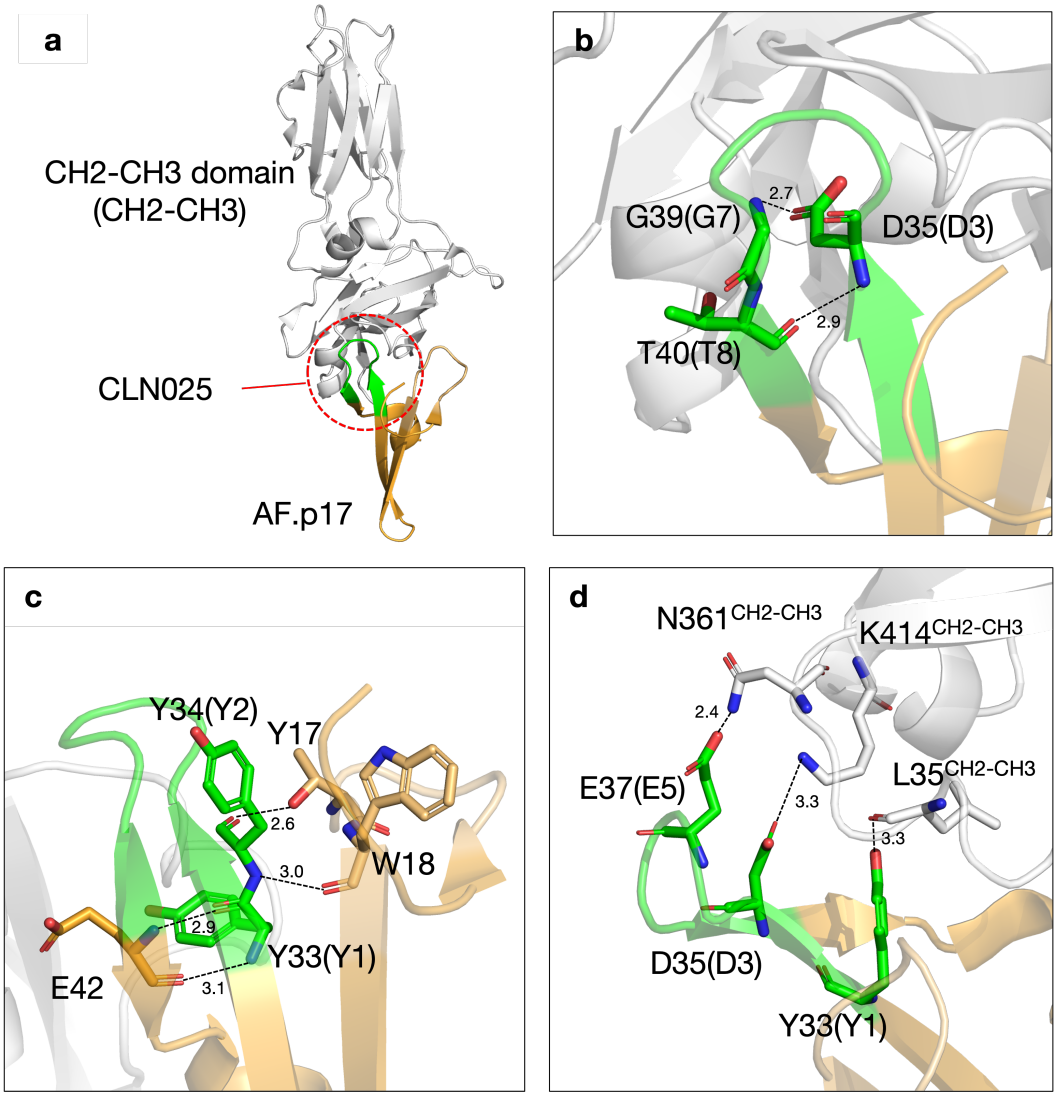

Fig. S20 (a)The structure of the AF.p17 and CH2-CH3 domain of the Fc region composite. (b-d) Non-covalent interactions of the assigned CLN025 fragment for (b)intramolecular interaction of CLN025, (c) intra- and (d) intermolecular interactions of AF.p17. The amino acids of the CLN025 fragments were shown in green. N and O atoms are colored in blue and red, respectively.

Table S1. Crystallographic data of **1-PhC**, **2-PhC**, **3-PhC**, **4-PhC**, and **2-PhC^{D74R}**.

	1-PhC	**2-PhC**	**3-PhC**	**4-PhC**	**2-PhC^{D74R}**
Data collection					
Space group	*I*23	*I*23	*I*23	*I*23	*I*23
Cell dimensions $a = b = c$ (Å)	104.53	104.52	104.82	104.59	104.11
Resolution range (Å)	50-1.55	50-1.75	50-1.70	50-1.85	50-1.70
	(1.56-1.55)	(1.76-1.75)	(1.71-1.70)	(1.87-1.85)	(1.76-1.70)
Observed reflections	17068904	4081869	27318402	3577789	8775836
	(281991)	(67144)	(435612)	(62678)	(147837)
Unique reflections	27659	19331	21218	16415	20807
	(674)	(489)	(508)	(414)	(527)
Redundancy	617.1	211.2	1287.5	218.0	421.8
	(418.4)	(137.3)	(857.5)	(151.4)	(280.5)
CC(1/2)	0.995	0.980	0.997	0.980	0.991
	(0.483)	(0.319)	(0.524)	(0.545)	(0.455)
I/σ(I)	10.3	5.8	12.6	6.1	8.1
	(1.3)	(1.2)	(1.5)	(1.6)	(1.4)
Completeness (%)	100.0	100.0	100.0	100.0	100.0
	(100.0)	(100.0)	(100.0)	(100.0)	(100.0)
Refinement					
Resolution (Å)	42.71-1.55	42.71-1.75	30.28-1.70	42.74-1.85	42.54-1.70
Number of reflections	24903	19931	19088	14790	18741
R-factor (%)	17.65	17.30	16.56	16.49	15.39
Free *R*-factor (%)	20.45	20.91	20.34	21.62	19.32
R. m. s. deviations					
Bond lengths (Å)	0.0114	0.0090	0.0102	0.0082	0.0100
Bond angles (°)	1.6951	1.5436	1.5812	1.4972	1.5844
Ramachandran plot (%)					
favoured	97.1	96.0	97.0	97.4	97.0
allowed	2.9	4.0	3.0	2.6	3.0
outlier	0.0	0.0	0.0	0.0	0.0

Values in parentheses are for the highest-resolution shell.

Table S2. Intra- and intermolecular interactions of the CLN025 fragment in **2-PhC**.

Bond type	Atoms of **CLN025$^{2\text{-PhC}}$**	Atoms of scaffold	Distance (Å)
Salt bridge	Oδ1/D74^{i}(D3)	Nζ/K66^{ii}	2.6
	Oε1/E76^{i}(E5)	Nζ/K66^{ii}	2.8
Hydrogen bond	Oδ1/D74^{i}(D3)	Nζ/K66^{ii}	2.6
	Oε1/E76^{i}(E5)	Nζ/K66^{ii}	2.8
	Oη/Y81^{i}(Y10)	Oδ2/D86^{iv}	2.3
	O/W80^{i}(W9)	N /D83^{iv}	3.3
	N/Y72^{i}(Y1)	O/K69^{i}	3.3
	N/Y73^{i}(Y2$^{)}$	O_{wat} –O/A67^{i}	3.1/2.8
	N/Y73^{i}(Y2)	O_{wat} –O/K69^{i}	3.1/2.8
	Oη/Y73^{i}(Y2)	Oε1/E63^{i}	2.5
	Oη/Y73^{i}(Y2)	Oε2/E63^{i}	3.3
	Oη/Y73^{i}(Y2)	Nη2/R214^{i}	3.3
	Oδ1/D74^{i}(D3)	O_{wat}–Oδ1/N217^{i}	3.1/3.5
	Oδ1/D74^{i}(D3)	O_{wat}–Nδ2/N91^{ii}	3.1/2.9
	Oδ2/D74^{i}(D3)	N/R218^{i}	3.3
	Oγ1/T77^{i}(T6)	Nη2/R218^{i}	2.7
SH---π interaction	Y73^{i}(Y2) aromatic ring	Sγ/C216^{i}	4.0
NH---π interaction	Y73^{i}(Y2) aromatic ring	Nη2/R214^{i}	4.1

Table S3. Non-covalent interactions of the CLN025 fragment in AF.p17 and **2-PhM**

	CLN025 (Y33–W41) in AF.p17			**CLN025$^{2\text{-PhC}}$** (Y72^{i}–Y81^{i}) in **2-PhM**		
	Bond pair	Bond type	Distance (Å)	Bond pair	Bond type	Distance (Å)
In fragment	D35(D3)/N-O/T40(T8)	Hydrogen bond	3.3	N/Y72^{i}(Y1)–O/Y73^{i}(Y2)	Hydrogen bond	3.5
	O/D35(D3)-N/G39(G7)	Hydrogen bond	2.7	O/D74^{i}(D3)–Oγ1/T77^{i}(T6)	Hydrogen bond	2.8
	Oδ2/D35(D3)–N/E37(E5)	Hydrogen bond	3.4	O/D74^{i}(D3)–N/T77^{i}(T6)	Hydrogen bond	3.2
	Oδ1/D35(D3)–Oγ1/T38(T6)	Hydrogen bond	3.3	O/P75^{i}(P4)–N/G78^{i}(G7)	Hydrogen bond	3.0
	Oγ1/T38(T6)–Oγ1/T40(T8)	Hydrogen bond	3.1	Oε2/E76^{i}(E5)–N/E76^{i}(E5)	Hydrogen bond	2.7
				O/G78^{i}(G7)–N/Y81^{i}(Y10)	Hydrogen bond	3.0
Intramolecular interactions	O/Y33(Y1)–N/E42	Hydrogen bond	2.9	N/Y72^{i}(Y1)–O/K69^{i}	Hydrogen bond	3.3
	N/Y33(Y1)–O/E42	Hydrogen bond	3.1	Oη/Y73^{i}(Y2)–Oε1/E63^{i}	Hydrogen bond	2.5
	N/Y34(Y2)–O/W18	Hydrogen bond	3.0	Oη/Y73^{i}(Y2)–Oε2/E63^{i}	Hydrogen bond	3.3
	O/Y34(Y2)–Oγ1/T17	Hydrogen bond	2.6	Oη/Y73^{i}(Y2)–Nη2/R214^{i}	Hydrogen bond	3.3
				Oδ2/D74^{i}(D3)–N/R218^{i}	Hydrogen bond	3.3
				Oγ1/T77^{i}(T6)–Nη2/R218^{i}	Hydrogen bond	2.7
				Y73^{i}(Y2) aromatic ring–Sγ/C216^{i}	SH---π interaction	4.0
				Y73^{i}(Y2) aromatic ring–Nη2/R214^{i}	NH---π interaction	4.1
Intermolecular interactions	Oη/Y33(Y1)–O/L358$^{CH2\text{-}CH3}$	Hydrogen bond	3.3	Oδ1/D74^{i}(D3)–Nζ/K66^{ii}	Salt bridge	2.6
	Oδ1/D35(D3)–Nζ/K414$^{CH2\text{-}CH3}$	Salt bridge	3.3	Oε1/E76^{i}(E5)–Nζ/K66^{ii}	Salt bridge	2.8
	Oε2/E37(E5)–Nδ2/N361$^{CH2\text{-}CH3}$	Hydrogen bond	2.4	Oη/Y81^{i}(Y10)	Oδ2/D86^{iv}	2.3
				O/W80^{i}(W9)	N/D83^{iv}	3.3

Reference

1. H. Mori, R. Ito, H. Nakazawa, M. Sumida, F. Matsubara and Y. Minobe, *J. Gen. Virol.*, 1993, **74**, 99-102.
2. K. Hirata, K. Yamashita, G. Ueno, Y. Kawano, K. Hasegawa, T. Kumasaka and M. Yamamoto, *Acta Crystallogr. Sect. D: Struct. Biol.*, 2019, **75**, 138-150.
3. C. Gati, G. Bourenkov, M. Klinge, D. Rehders, F. Stellato, D. Oberthur, O. Yefanov, B. P. Sommer, S. Mogk, M. Duszenko, C. Betzel, T. R. Schneider, H. N. Chapman and L. Redecke, *IUCrJ*, 2014, **1**, 87-94.
4. K. Hasegawa, K. Yamashita, T. Murai, N. Nuemket, K. Hirata, G. Ueno, H. Ago, T. Nakatsu, T. Kumasaka and M. Yamamoto, *J. Synchrotron Rad.*, 2017, **24**, 29-41.
5. A. J. M. Duisenberg, *J. Appl. Crystallogr.*, 1992, **25**, 92-96.
6. H. R. Powell, O. Johnson and A. G. W. Leslie, *Acta Crystallogr. Sect. D: Biol. Crystallogr.*, 2013, **69**, 1195-1203.
7. T. A. White, V. Mariani, W. Brehm, O. Yefanov, A. Barty, K. R. Beyerlein, F. Chervinskii, L. Galli, C. Gati, T. Nakane, A. Tolstikova, K. Yamashita, C. H. Yoon, K. Diederichs and H. N. Chapman, *J. Appl. Crystallogr.*, 2016, **49**, 680-689.
8. P. V. Afonine, R. W. Grosse-Kunstleve, N. Echols, J. J. Headd, N. W. Moriarty, M. Mustyakimov, T. C. Terwilliger, A. Urzhumtsev, P. H. Zwart and P. D. Adams, *Acta Crystallogr. Sect. D: Struct. Biol.*, 2012, **68**, 352-367.
9. P. Emsley and K. Cowtan, *Acta Crystallogr. Sect. D: Struct. Biol.*, 2004, **60**, 2126-2132.
10. S. C. Lovell, I. W. Davis, W. B. Arendall, 3rd, P. I. de Bakker, J. M. Word, M. G. Prisant, J. S. Richardson and D. C. Richardson, *Proteins*, 2003, **50**, 437-450.
11. W. L. Jorgensen, J. Chandrasekhar, J. D. Madura, R. W. Impey and M. L. Klein, *J. Chem. Phys.*, 1983, **79**, 926-935.
12. J. A. Maier, C. Martinez, K. Kasavajhala, L. Wickstrom, K. E. Hauser and C. Simmerling, *J. Chem. Theory Comput.*, 2015, **11**, 3696-3713.
13. R. T. McGibbon, K. A. Beauchamp, M. P. Harrigan, C. Klein, J. M. Swails, C. X. Hernandez, C. R. Schwantes, L. P. Wang, T. J. Lane and V. S. Pande, *Biophys. J.*, 2015, **109**, 1528-1532.